Journal of Power Sources 375 (2018) 131–137

Contents lists available at ScienceDirect

Journal of Power Sources

journal homepage: www.elsevier.com/locate/jpowsour

Mechanistic elucidation of thermal runaway in potassium-ion batteries

Ryan A. Adams, Arvind Varma, Vilas G. Pol*

Davidson School of Chemical Engineering, Purdue University, West Lafayette, IN 47907, United States

HIGHLIGHTS

- Thermal runaway from K-ion graphite anode initiates at 100 °C.
- 63% less total heat is generated for the K-ion system as compared to Li-ion.
- Consumption of all intercalated K occurs by 150 °C, fueling the peak at 100 °C.
- K-ion SEI manipulation can mitigate this by preventing graphite-electrolyte contact.

GRAPHICAL ABSTRACT

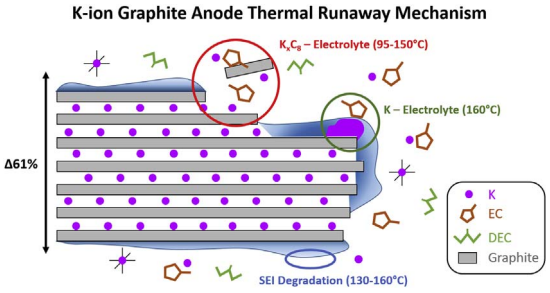

ARTICLE INFO

Keywords:
Potassium-ion batteries
Thermal runaway
Differential scanning calorimetry
Graphite anode

ABSTRACT

For the first time, thermal runaway of charged graphite anodes for K-ion batteries is investigated, using differential scanning calorimetry (DSC) to probe the exothermic degradation reactions. Investigated parameters such as state of charge, cycle number, surface area, and binder demonstrate strong influences on the DSC profiles. Thermal runaway initiates at 100 °C owing to K_xC_8 – electrolyte reactions, but the K-ion graphite anode evolves significantly less heat as compared to the analogous Li-ion system (395 J g^{-1} vs. 1048 J g^{-1}). The large volumetric expansion of graphite during potassiation cracks the SEI layer, enabling contact and reaction of KC_8 – electrolyte, which diminishes with cycle number due to continuous SEI growth. High surface area graphite decreases the total heat generation, owing to thermal stability of the K-ion SEI layer. These findings illustrate the dynamic nature of K-ion thermal runaway and its many contrasts with the Li-ion graphite system, permitting possible engineering solutions for safer batteries.

1. Introduction

Safety remains a primary concern of lithium ion batteries (LIBs) despite more than two decades of commercialization and widespread usage [1,2]. Thermal runaway can initiate from exothermic breakdown of the SEI layer on carbon anodes, which starts typically at 120 °C [3–5]. Heat generation from electrolyte breakdown and reaction with lithiated carbon leads to cathode decomposition and release of oxygen, increasing system pressure and reactivity [6–8]. By 200 °C, total exothermic heat generation of 2 kJ g^{-1} electrode material occurs, resulting in intense explosions and flames [9]. Evolution of CO_2, O_2, H_2, POF_3, and HF from decomposition reactions of electrolyte, salt, polymer binder, and electrodes contributes to increased heat and pressure, accelerating the process [10]. As the initiating process for thermal runaway of LIBs, the degradation reactions of SEI breakdown are of great interest to understand and mitigate [11]. Factors including state of charge (SOC), electrolyte composition, binder, and carbon material properties significantly impact thermal runaway [3]. Various strategies, including alternative binders, electrolyte components, and flame retardant additives, can mitigate heat generation in the Li-ion battery system, but typically adversely affect electrochemical performance [12,13]. In practice, LIBs must be carefully designed and regulated for

* Corresponding author.
E-mail address: vpol@purdue.edu (V.G. Pol).

https://doi.org/10.1016/j.jpowsour.2017.11.065
Received 20 October 2017; Received in revised form 10 November 2017; Accepted 21 November 2017

safe operation, leading to manufacturing cost increases for failsafe mechanisms (gas relief valves, safety vents, etc.) and rigorous testing by heating, short-circuiting, overcharging, nail puncturing, and crushing of cells [9].

Recently, non-aqueous potassium-ion batteries (KIBs) have received interest as a novel energy storage technology, utilizing inexpensive and abundant potassium as the charge carrier ion. KIBs operate in a manner similar to LIBs, with K ion intercalation between cathode and anode through an organic solvent-inorganic salt electrolyte medium [14,15]. Despite its larger ionic size, KIBs have an advantage over its competitor, the sodium-ion battery, as K ions can electrochemically intercalate into graphite to form stage-one KC_8 structure for 279 mAh g^{-1}, whereas Na is limited to NaC_{64} for 35 mAh g^{-1} [16,17]. Formation of KC_8 causes 61% volumetric expansion of graphite however, resulting in electrode pulverization and excessive solid electrolyte interphase (SEI) formation over time [17,18]. Utilization of functionalized binders, such as sodium carboxymethylcellulose (CMCNa), and optimized electrolyte significantly improve electrochemical performance, with increased first cycle Coulombic efficiency and long-term cycling stability [19,20]. Many carbon materials have been evaluated for KIB anodes, including hard carbon microspheres, carbon nanofibers, F- or N-doped graphene, polynanocrystalline graphite, and tire-derived hard carbon [21–27]. The expanded graphitic interlattice spacing mitigates electrode pulverization induced by volumetric changes, resulting in exceptional rate capability and cycling stability. Several KIB cathode materials have shown promising performance, including layered K metal oxide materials, such as $K_{0.3}MnO_2$, $K_{0.7}Fe_{0.5}Mn_{0.5}O_2$, and $K_{0.6}CoO_2$, as well as vanadium phosphate $KVPO_4F$ and $KVOPO_4$ [28–31]. Despite this exceptional electrochemical performance, no prior studies have been reported regarding KIB carbon anode safety to evaluate the practicality of this novel battery system.

Possible safety concerns for KIBs arise from several aspects: (1) Potassium metal is dangerous due to its formation of highly reactive superoxide compounds. (2) K metal melts at 63.5 °C, as compared to 97.8 °C for Na and 180.5 °C for Li. (3) Stage-one KC_8 is pyrophoric. (4) An organic based electrolyte is utilized, making the system flammable and self-sustaining in exothermic breakdown reactions. While K metal anode is not utilized per se in the full cell, the possibility of K metal deposition and plating on the carbon anode remains. Additionally, properties of the K-ion SEI layer remain largely unknown, although some studies have predicted it to be more stable than Li-ion and Na-ion SEI with increased fraction of inorganic salts, such as K_2CO_3 [32–34]. In this study, graphite is the primary electrode material investigated, due to its favorable energy density, voltage plateau, and commercialization viability. Differential scanning calorimetry (DSC) is the primary technique used to study the KIB graphite system, with selective sample preparation to determine the thermal runaway mechanism and heat generation in comparison to LIBs. To our knowledge, this is the first study to explore safety aspects of KIBs, analyze thermal runaway of graphite anode, and evaluate its practicality for commercialization.

2. Experimental

Electrodes were prepared with a ratio of 80 wt. % active material (e.g. synthetic graphite), 10 wt. % conductive additive (Timcal Super C65), and 10 wt. % polymer binder (polyvinylidene fluoride). Using N-methyl-2-pyrrolidone as solvent, a slurry was mixed for 20 min and tape-cast onto aluminum foil via doctor-blade. For laminates constructed with functionalized binders, such as CMCNa or Na-alginate, water was utilized as solvent. The laminate was dried for 12 h in a vacuum oven set to 80 °C, and then 12 mm diameter electrodes were punched out with an active material density of ~2.5 mg cm^{-2}. Electrochemical tests were performed in a coin-type 2032 half-cell, using potassium metal as the counter and reference electrode. Whatman 934-AH glass microfiber was used as separator and 0.8 M KPF_6 in a 1:1 (by volume) mixture of ethylene carbonate (EC)/diethyl carbonate (DEC) was utilized as electrolyte. Galvanostatic cycling was performed with an Arbin cycler in a voltage range of 0.005–1.5 V at room temperature. To condition for differential scanning calorimetry (DSC) analysis, half-cells were cycled at C/10 current density (determined by theoretical capacity of 279 mAh g^{-1}, according to KC_8 stage-one structure) for 5 cycles for the base case, with the corresponding voltage set at equilibrium condition (< 1 μA current). To remove electrolyte, the electrode was washed with dimethyl carbonate (DMC) three times, with vacuum drying in-between. Lithium-ion coin cells were prepared using copper-foil cast graphite electrodes, with Li metal as the counter electrode, Celgard 2500 as separator, and 1 M $LiPF_6$ in 1:1 (by volume) EC/DEC.

DSC was performed with a TA Instruments Q20 instrument, at a scan rate of 5 °C min^{-1}. To perform DSC analysis, the conditioned coin cell was dissembled in an argon glovebox, with the potassiated electrode material scraped off the current collector into a hermetically sealed aluminum pan. A Mettler Toledo XS3DU microbalance was used to precisely measure mass loading of wetted electrode material, with an average 1–2 mg sample size. Low mass loading was used to prevent gassing and breakage of the hermetic seal at higher temperatures due to electrolyte evaporation, and results showing irregular jumps or weight loss after DSC measurements were removed. To ensure consistency of results, multiple coin cells were constructed for each trial, with 2 samples run from each individual electrode, and representative data is provided in this study. Scanning electron microscopy (FE-SEM) images were recorded using a Hitachi S-4800 microscope. Powder X-ray diffraction (XRD) was utilized to characterize the crystalline phase via the Bragg – Brentano method (Rigaku SmartLab X-ray diffractometer). A Cu-Kα X-ray source (λ = 0.154 184 nm) was used to obtain the XRD patterns (2θ = 5–80°) at a scanning rate of 2° min^{-1} with samples sealed by Kapton tape. Raman spectra were collected with a 633 nm laser utilizing a Thermo Scientific DXR Raman microscope and an inert sample holder loaded in an argon glovebox. Surface area analysis (Quantachrome Instruments NOVA 2200e) was conducted using nitrogen adsorption/desorption isotherm measurements at 77 K. Samples were degassed for 12 h at 300 °C prior to measurements. Multipoint specific surface area calculations were performed using the linear portion (P/P_0 = 0.05–0.30) of the Brunauer – Emmett – Teller (BET) model. Stage-one KC_8 was chemically synthesized by taking stoichiometric ratios of graphite and K metal, and heating in an inert atmosphere under stirring at 200 °C for 2 h. High surface area graphite was produced by ball milling (Quantachrome Instruments MillPrep-Micro Ball Mill) for either 1 or 5 h, followed by particle sieving (Endecotts > 25 μm & < 53 μm stainless steel sieve) to improve particle size homogeneity.

3. Results and discussion

A typical second cycle charge-discharge voltage profiles for a graphite anode tested in Li-ion and K-ion systems are shown in Fig. 1. At 20 mA g^{-1}, the graphite anode achieves close to the theoretical capacities of 279 mAh g^{-1} for KC_8 and 372 mAh g^{-1} for LiC_6. The higher intercalation potential of K versus Li reduces the risk of plating and dendrite formation on the anode, which can occur at very low potentials, high currents, and low operating temperatures [35]. The first cycle voltage profile is shown in Fig. S1a, where the K-ion system has a Coulombic efficiency of 43%, as compared to 80% for Li-ion, likely occurring due to excessive SEI formation from the 61% volume expansion during potassiation [17]. Extended galvanostatic cycling, as shown in Fig. S1b, reveals a capacity fade of 35% over 50 cycles for the K-ion graphite anode, due to electrode pulverization and SEI buildup as signified by 95% average Coulombic efficiency. In contrast, the Li-ion graphite anode shows rapid stabilization and 99.9% average Coulombic efficiency over 50 cycles. The synthetic graphite material properties are characterized in Fig. S2, with Raman spectrum, XRD pattern, SEM imaging, and N_2 sorption isotherms, giving a BET surface area